

PHYSICS

Molecular engineering of Rashba spin-charge converter

Hiroyasu Nakayama,¹ Takashi Yamamoto,² Hongyu An,¹ Kento Tsuda,²
Yasuaki Einaga,² Kazuya Ando^{1*}

In heterostructures with broken inversion symmetry, the electrons' motion is coupled to their spin through interface-driven spin-orbit coupling: the Rashba effect. The Rashba effect enables the interconversion between spin and charge currents, offering a variety of novel spintronic phenomena and functionalities. However, despite the significant progress in Rashba physics, controlling the spin-charge conversion in metallic heterostructures remains a major challenge. We show that molecular self-assembly provides a way to engineer the Rashba spin-charge converters. We demonstrate that magnetoresistance and voltage generation originating from the spin-charge conversion in metallic heterostructures can be manipulated by decorating the surface with self-assembled organic monolayers through the cooperative molecular field effect. We also demonstrate reversible phototuning of the spin-charge conversion through light-driven molecular transformations using a molecule that can photoisomerize between the trans and cis states. These findings, with the almost-infinite chemical tunability of organic monolayers, pave the way toward molecular engineering of spin-orbit devices.

INTRODUCTION

Spin-orbit coupling (SOC) in solids plays a crucial role in modern spintronics (1–7). A typical example of SOC effects is the conversion between charge and spin currents. When a charge current passes through a heavy metal with strong SOC, electrons with opposite spins are deflected in opposite directions, resulting in the generation of a transverse spin current (8–10). This charge-spin conversion, the spin Hall effect, and its inverse are responsible for a variety of spintronic phenomena and functionalities, such as the spin-torque magnetization switching and spin-Seebeck thermoelectric conversion (11). SOC effects are enhanced in reduced dimensions: two-dimensional electron gases (2DEGs) that exist at surfaces, at interfaces, or in semiconductor quantum wells (6, 7). In such systems, inversion symmetry is broken, and the resultant electric field couples to the spin of itinerant electrons, which is known as Rashba SOC (12). The Rashba SOC produces spin-split dispersion and locks spin to the momentum. Because of the spin-momentum locking, a charge flow in a Rashba 2DEG results in the creation of a non-zero spin polarization (13), providing an alternative way for the charge-spin conversion (see Fig. 1A). Although this phenomenon, the Rashba-Edelstein effect, was first observed in semiconductors (14), it is now intensively studied in metallic heterostructures; the Rashba-Edelstein effect and its inverse appear to offer an efficient way for the conversion between charge and spin currents in metallic spin-orbit devices (6, 7, 15).

An attractive aspect of the Rashba SOC is its ability to be controlled externally, which has been the heart of semiconductor spintronics (6, 7). Because the strength of the Rashba SOC is directly related to the interfacial potential drop in semiconductor heterostructures, the controlled magnitude of the Rashba SOC can be realized by applying a gate voltage, which modifies the quantum well asymmetry and electron occupation. In contrast to semiconductors, however, the electronic properties of metals are difficult to be changed significantly. Thus, despite the recent extensive studies on metal spintronics, tuning the conversion between charge and spin currents in metallic Rashba spin-orbit devices remains a major challenge.

Here, we demonstrate that the charge-spin conversion in metallic Rashba spin-orbit devices can be controlled by molecular self-assembly (16–21). We show that the decoration of self-assembled organic monolayers (SAMs) on Bi/Ag/CoFeB trilayers changes the strength of the Rashba-Edelstein effect at the Bi/Ag interface, where the Rashba SOC is two orders of magnitude larger than in semiconductor heterostructures (22). We further demonstrate reversible phototuning of the Rashba-Edelstein effect through light-driven molecular transformations using an azobenzene (AZ)-functionalized SAM, which can reversibly isomerize between trans and cis forms under photoirradiation. These results, with a high degree of tunability and versatility of organic chemistry, promise a way to create organic-inorganic hybrid systems where molecular properties are integrated into spin-orbit devices.

RESULTS

Molecular engineering of Rashba-Edelstein magnetoresistance

The chemically tailored Rashba-Edelstein effect is evidenced by measuring the Rashba-Edelstein magnetoresistance (REMR). The REMR refers to the magnetoresistance induced by the Rashba SOC and spin-current reflection (23). As shown in Fig. 1B, in a Bi/Ag/CoFeB trilayer, a spin accumulation generated from a 2D charge current through the Rashba-Edelstein effect diffuses as a 3D spin current in the Ag layer. The spin current is reflected at the Ag/CoFeB interface and is then converted into a 2D charge current through the inverse Rashba-Edelstein effect. This process generates an additional charge current, changing the electrical resistance of the trilayer, which is the REMR. The Bi(5 nm)/Ag(2 nm)/CoFeB(2.5 nm) trilayers used in this study were deposited on Gd₃Ga₅O₁₂ (GGG) (111) single crystalline substrates at room temperature by radio frequency magnetron sputtering with a base pressure of around 3×10^{-6} Pa. The numbers in parentheses represent the thickness. To study the effect of the decoration of organic monolayers on the Rashba spin-orbit device, we used 2 mM solutions 1-octadecanethiol (ODT) and 1*H*,1*H*,2*H*,2*H*-perfluorodecanethiol (PFDT) in ethanol to form SAMs on the Bi/Ag/CoFeB trilayers (for details, see Methods). As expected for the SAM-decorated surface, the water contact angle of the Bi/Ag/CoFeB trilayer increases after the SAM formation, as shown in Fig. 1C. The SAM formation is further confirmed by the change in the work function Φ of the Bi/Ag/CoFeB

Copyright © 2018
The Authors, some
rights reserved;
exclusive licensee
American Association
for the Advancement
of Science. No claim to
original U.S. Government
Works. Distributed
under a Creative
Commons Attribution
NonCommercial
License 4.0 (CC BY-NC).

¹Department of Applied Physics and Physico-Informatics, Keio University, Yokohama 223-8522, Japan. ²Department of Chemistry, Keio University, Yokohama 223-8522, Japan.

*Corresponding author. Email: ando@appi.keio.ac.jp

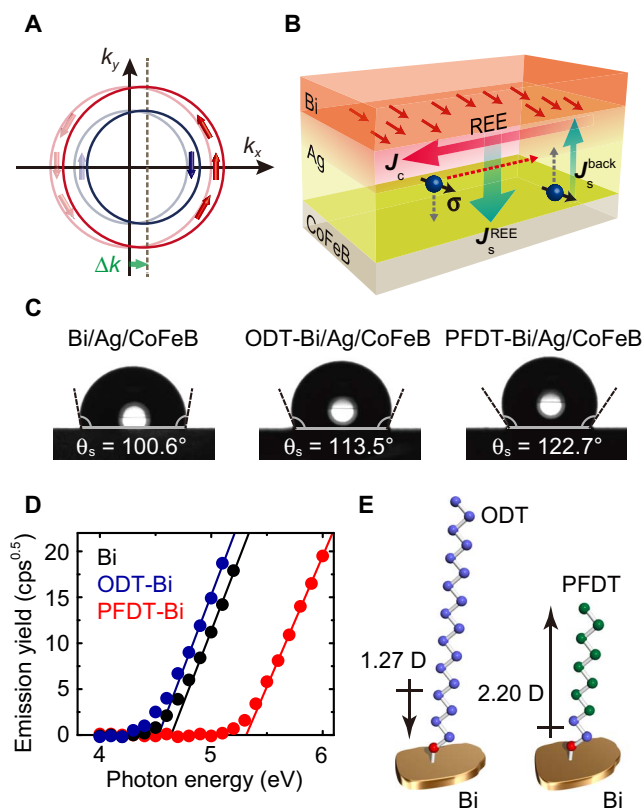


Fig. 1. Rashba spin-orbit device decorated with SAMs. (A) Fermi contours of a Rashba system under an external electric field. A shift of the Fermi circles gives rise to a spin polarization. (B) Schematic illustration of the REMR in a Bi/Ag/CoFeB trilayer induced by the Rashba-Edelstein effect at the Bi/Ag interface. (C) The static water contact angles θ_s of the Bi/Ag/CoFeB trilayers measured by putting 1.5 μ l of a water droplet on the surface. (D) Square root of photoelectron emission yield as a function of scan energy measured with an atmospheric photoelectron spectrometer for the pristine Bi/Ag/CoFeB trilayer (black), Bi/Ag/CoFeB trilayer decorated with ODT (blue), and Bi/Ag/CoFeB trilayer decorated with PFDT (red). The solid lines are linear fits, from which the baseline intercept gives the work function of the trilayers. (E) Schematic illustration of ODT and PFDT molecules on the Bi surface. The arrows represent the dipole moment of the SAM-forming molecules obtained from DFT calculations.

trilayer measured with an atmospheric photoelectron spectrometer (see Fig. 1D). Figure 1D shows that the ODT formation decreases Φ , whereas the PFDT formation increases Φ . Because the change in the metal work function due to the molecular self-assembly is associated with the dipole moment of the SAM-forming molecule perpendicular to the surface (17), the change in Φ shows that ODT and PFDT have opposite dipoles, consistent with density functional theory (DFT) calculations (see Fig. 1E and Methods). The SAM-decorated surfaces were further characterized using the atomic force microscopy (AFM) and infrared reflection-absorption spectroscopy (IRRAS) (see the Supplementary Materials). These results indicate homogeneous and well-packed formation of the SAMs on the Bi surface. The SAM formation on the Bi surface, confirmed by the contact angle, work function, and IRRAS measurements, shows that oxide formation at the SAM-Bi interfaces can be neglected. Although the surface of the Bi layer can be oxidized before the self-assembly, the oxide formed on the Bi surface is reduced to metallic Bi by the redox reaction between the metal oxide and thiols during the SAM formation process; the oxide is reduced upon the

oxidation of the thiols to disulfides (24). The absence of the oxidized layer at the SAM-Bi interfaces is also supported by the AFM images showing smooth surface and low surface roughness of the SAM-decorated Bi/Ag/CoFeB, which are consistent with the previous report (24).

Figure 2 (A to C) shows the change in the longitudinal resistance, ΔR , of the Bi/Ag/CoFeB trilayers during rotation of an applied magnetic field $\mu_0 H = 6$ T in the xy , zy , and zx planes. The rotation angles (α , β , and γ) are defined in Fig. 2D. At $\mu_0 H = 6$ T, the magnetization M of the CoFeB layer is saturated and oriented parallel to H . As shown in Fig. 2A, we observed a field angle-dependent MR (ADMR) in all three orthogonal planes for the pristine Bi/Ag/CoFeB trilayer. $\Delta R(\beta)$ is of particular importance. In the Bi/Ag/CoFeB trilayer, the anisotropic MR (AMR) of the CoFeB layer contributes to the ADMR. The AMR phenomenology predicts $\Delta R(\alpha) \sim \cos^2 \alpha$, $\Delta R(\gamma) \sim \sin^2 \gamma$, and $\Delta R(\beta) = 0$. Although $\Delta R(\beta) \sim \sin^2 \beta$ can be induced by the geometrical size effect of the AMR (25), the observed symmetry, $\Delta R(\beta) \sim -\sin^2 \beta$, is different from the prediction of the AMR phenomenology. Another possible source of the ADMR in the Bi/Ag/CoFeB trilayer is the REMR arising from the Rashba-Edelstein effect at the Bi/Ag interface. The REMR resistivity can be expressed as $\rho = \rho_0 - \Delta\rho_{Rm_y^2}$, where ρ_0 is a constant resistivity offset, m_y is the y component of the unit vector of M , and $\Delta\rho_R$ is the magnitude of the resistivity change due to the REMR (23). Thus, the REMR predicts $\Delta R(\beta) \sim -\sin^2 \beta$, which is consistent with the $\Delta R(\beta)$ result shown in Fig. 2A. Therefore, the observed ADMR, $\Delta R(\beta)$, can be attributed to the REMR in the Bi/Ag/CoFeB trilayer. This interpretation has been further supported by Ag layer thickness and field strength dependence of the MR in the Bi/Ag/CoFeB trilayer (23).

Our finding is that the strength of the REMR can be tuned by the molecular self-assembly on the Rashba spin-orbit device. In Fig. 2 (B and C), we show the ADMR for the Bi/Ag/CoFeB trilayers decorated with ODT and PFDT, respectively. Figure 2B shows that the amplitude of $\Delta R(\beta)$ is enhanced by decorating the surface of the Bi/Ag/CoFeB trilayer with ODT. In contrast, as shown in Fig. 2C, the amplitude of $\Delta R(\beta)$ is suppressed by the SAM formation of PFDT. Here, we note that $\Delta R(\gamma)$ is not affected by the SAM formations (see Fig. 2, A to C). In the trilayer, $\Delta R(\gamma)$ is purely induced by the AMR in the CoFeB layer because the REMR predicts $\Delta R(\gamma) = 0$. Thus, the negligible change in $\Delta R(\gamma)$ shows that the AMR in the CoFeB layer is not influenced by the surface decoration of the trilayer with ODT and PFDT. In contrast to $\Delta R(\gamma)$, $\Delta R(\alpha)$ and $\Delta R(\beta)$ in the trilayer can be induced by both the AMR and REMR. The negligible change in the AMR after the SAM formation demonstrates that the observed change in $\Delta R(\alpha)$ and $\Delta R(\beta)$ originates from the modulation of the REMR induced by the molecular self-assembly (see also the Supplementary Materials).

The observed change in the REMR due to the molecular self-assembly originates from charge transfer at the organic-inorganic interface in the SAM-decorated spin-orbit devices. Figure 2 (B and C) shows that the REMR in the trilayer can be either enhanced or suppressed, depending on the direction of the dipole moment of the SAM-forming molecules (see also Fig. 1, D and E). When the SAMs are formed on the Bi surface, charge redistribution appears between the molecules and Bi through the cooperative molecular field effect (26). This charge transfer at the interface alters the bulk electronic properties of the Bi layer due to the long screening length of Bi, ~ 30 nm (27), and thus, the potential drop at the Bi/Ag interface is affected by the SAM formation. It is notable that the direction of the charge transfer between the molecules and Bi is opposite at the ODT-Bi and PFDT-Bi interfaces because of the opposite direction of the dipole moment (28). This results in the enhanced or suppressed Rashba-Edelstein effect at

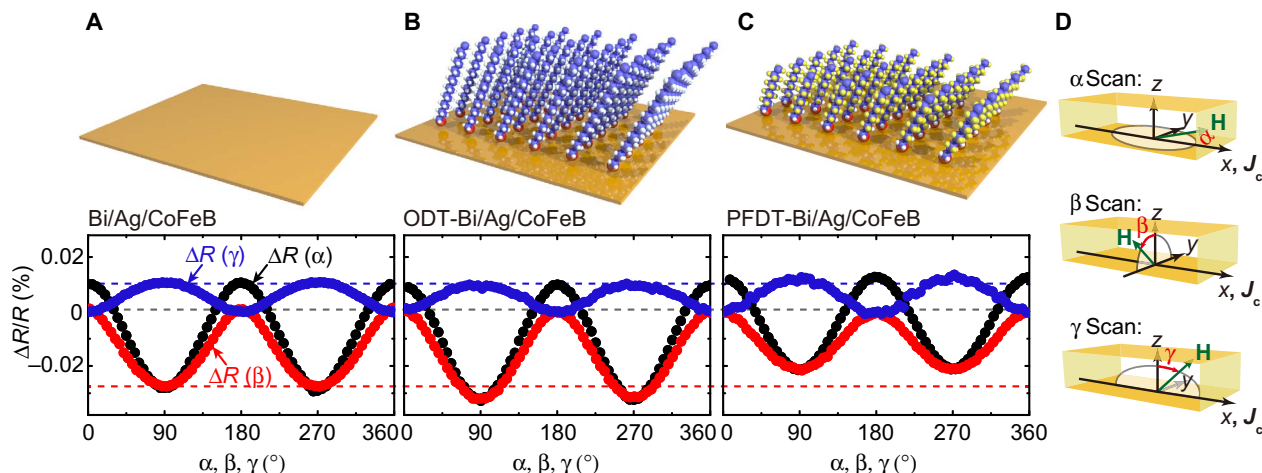


Fig. 2. Rashba-Edelstein MR. The change in the longitudinal resistance, ΔR , of (A) the Bi(5 nm)/Ag(2 nm)/CoFeB(2.5 nm) trilayer, (B) ODT-Bi(5 nm)/Ag(2 nm)/CoFeB(2.5 nm) trilayer, and (C) PFDT-Bi(5 nm)/Ag(2 nm)/CoFeB(2.5 nm) trilayer, as a function of the rotation of the magnetic field of 6 T, where R is the longitudinal resistance at $\mu_0 H = 0$. The rotation angles (α , β , and γ) are defined in (D). The schematic illustrations of the pristine Bi/Ag/CoFeB trilayer and SAM-decorated Bi/Ag/CoFeB trilayers are also shown. The schematic illustrations of the SAMs were drawn based on the literature (39), where an n -alkyl thiol molecule forms SAM tilted from the surface normal by 20° to 30° . Although this case is for SAM on gold, DFT and AM1 calculations have shown that the molecular configuration on bismuth is similar to that on gold (40).

the Bi/Ag interface, depending on the direction of the charge transfer or the direction of the dipole moment of the SAM-forming molecules (see also the Supplementary Materials). Although the charge transfer at the interface can also change the electrical resistance of the Bi layer, the change in the REMR by the SAM formation cannot be attributed to a possible change in the charge-current distribution in the trilayer caused by the resistance change. We have confirmed that the change of the longitudinal resistance R of the trilayer at $\mu_0 H = 0$ due to the SAM formations is only a few percent: $(R_{\text{ODT-Bi/Ag/CoFeB}} - R_{\text{Bi/Ag/CoFeB}})/R_{\text{Bi/Ag/CoFeB}} = -1.1\%$ and $(R_{\text{PFDT-Bi/Ag/CoFeB}} - R_{\text{Bi/Ag/CoFeB}})/R_{\text{Bi/Ag/CoFeB}} = -3.0\%$, which is negligible compared to the change of the MR ratio shown in Fig. 2: $(MR_{\text{ODT-Bi/Ag/CoFeB}} - MR_{\text{Bi/Ag/CoFeB}})/MR_{\text{Bi/Ag/CoFeB}} = 14\%$ and $(MR_{\text{PFDT-Bi/Ag/CoFeB}} - MR_{\text{Bi/Ag/CoFeB}})/MR_{\text{Bi/Ag/CoFeB}} = -26\%$, where $MR \equiv [\Delta R(\beta = 0) - \Delta R(\beta = 90^\circ)]/R$. The negligible change in the electrical resistance shows that the distribution of the applied charge current in the trilayer is not affected by the SAM formation. The negligible change in the current distribution is consistent with the fact that most of the applied charge current flows in the low-resistivity Ag layer, which is not affected by the SAM formation due to the very short screening length, ~ 0.06 nm (29). This result further supports that the change in the strength of the Rashba-Edelstein effect at the Bi/Ag interface is responsible for the observed change in the REMR caused by the SAM formation.

Spin pumping and inverse Rashba-Edelstein effect

The molecular engineering of the conversion between charge and spin currents at the Rashba interface is further evidenced by measuring the inverse Rashba-Edelstein effect using the spin pumping. The spin pumping in a Bi/Ag/Ni₈₁Fe₁₉ trilayer injects a spin current into the Bi/Ag junction from the Ni₈₁Fe₁₉ layer under ferromagnetic resonance (FMR) (30). The injected spin current induces a nonzero spin density at the Bi/Ag interface, generating a charge current through the spin-momentum locking of the interfacial Rashba states: the inverse Rashba-Edelstein effect (31). To measure the inverse Rashba-Edelstein effect induced by spin pumping, we placed the Bi/Ag/Ni₈₁Fe₁₉ trilayer at the center of a TE₀₁₁ microwave cavity with a resonance frequency of $f = 9.44$ GHz. We measured dc electric voltage V between electrodes

attached to the edges of the film by applying an in-plane external magnetic field $\mu_0 H$ perpendicular to the direction across the electrodes at room temperature (32).

Figure 3 (A and B) shows the $\mu_0 H$ dependence of the charge current J_c measured for a Ag/Ni₈₁Fe₁₉ bilayer and the Bi/Ag/Ni₈₁Fe₁₉ trilayer, respectively, where $J_c = V/R$ and R is the resistance of the films. The J_c spectra show that the J_c signal in the Bi/Ag/Ni₈₁Fe₁₉ trilayer is significantly larger than that in the Ag/Ni₈₁Fe₁₉ bilayer, in which the Bi layer is missing, showing that the Bi/Ag interface plays an essential role in the J_c generation. This result indicates that the origin of the J_c signal observed in the Bi/Ag/Ni₈₁Fe₁₉ trilayer can be attributed to the inverse Rashba-Edelstein effect at the Bi/Ag interface. By fitting the measured J_c spectra using a combination of symmetric $J_{\text{sym}}(H) = J_{\text{sym}}\Gamma^2/[(H - H_{\text{FMR}})^2 + \Gamma^2]$ and antisymmetric $J_{\text{asym}}(H) = J_{\text{asym}}[-2\Gamma(H - H_{\text{FMR}})]/[(H - H_{\text{FMR}})^2 + \Gamma^2]$ functions (32), $J(H) = J_{\text{sym}}(H) + J_{\text{asym}}(H)$, we found that the magnitude of the symmetric component J_{sym} of the J_c signal in the Bi/Ag/Ni₈₁Fe₁₉ trilayer is orders of magnitude larger than that in the Ag/Ni₈₁Fe₁₉ bilayer, whereas the magnitude of the antisymmetric component J_{asym} is comparable in these films as shown in Fig. 3 (A and B), where $\mu_0 H_{\text{FMR}}$ is the resonance field and Γ denotes the linewidth. This is consistent with the fact that the symmetric component of J_c is attributed to the spin-to-charge conversion induced by the spin pumping, whereas the antisymmetric component is attributed to magnetogalvanic effects in the ferromagnetic layer (32). These observations led us to the conclusion that the J_s signal observed for the Bi/Ag/Ni₈₁Fe₁₉ trilayer is dominated by the charge current generated by the inverse Rashba-Edelstein effect induced by spin pumping.

The amount of charge current generated by the inverse Rashba-Edelstein effect can be tuned by the molecular self-assembly on the Bi/Ag/Ni₈₁Fe₁₉ trilayer. In Fig. 3 (C and D), we show the J_c spectra measured for the Bi/Ag/Ni₈₁Fe₁₉ trilayers decorated with ODT and PFDT, respectively. These results show that the magnitude of the antisymmetric component of the J_c signals is almost unchanged by the decoration of the SAMs. This is consistent with the fact that the antisymmetric signal is generated in the Ni₈₁Fe₁₉ layer, which is not influenced by the surface decoration of the trilayer with the SAMs. In contrast to the negligible change in the antisymmetric component,

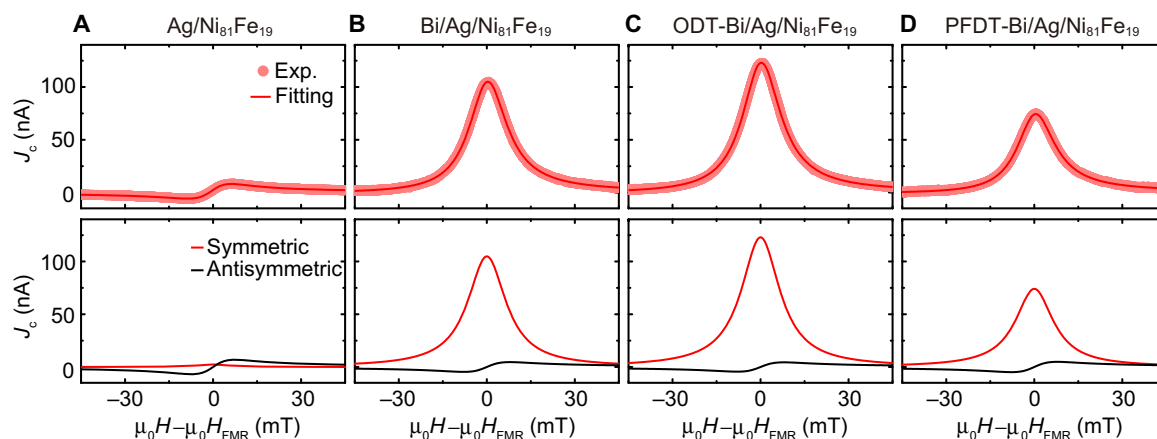


Fig. 3. Spin pumping and inverse Rashba-Edelstein effect. Magnetic field μ_0H dependence of the charge current J_c , derived from the dc electric voltage, for the (A) Ag(2.5 nm)/Ni₈₁Fe₁₉(6 nm), (B) Bi(5 nm)/Ag(2.5 nm)/Ni₈₁Fe₁₉(6 nm), (C) ODT-Bi(5 nm)/Ag(2.5 nm)/Ni₈₁Fe₁₉(6 nm), and (D) PFDT-Bi(5 nm)/Ag(2.5 nm)/Ni₈₁Fe₁₉(6 nm) films measured by applying a 200-mW microwave, where μ_0H_{FMR} is the FMR field. The solid circles are the experimental data, and the solid curves are the fitting result using a combination of symmetric and antisymmetric functions. The symmetric and antisymmetric components of the fitting results are plotted correspondingly.

the magnitude of the symmetric component is enhanced by decorating the surface of the Bi/Ag/Ni₈₁Fe₁₉ trilayer with ODT. The change in the symmetric component is reversed by the PFDT formation; the magnitude of the symmetric component is suppressed by decorating the surface with PFDT, as shown in Fig. 3D. These results are consistent with the change in the REMR due to the molecular self-assembly; the ODT(PFDT) formation enhances(suppresses) the REMR. The observed tuning of the inverse Rashba-Edelstein effect induced by the spin pumping, as well as the REMR, illustrates the generality and versatility of the molecular engineering of the Rashba devices.

Reversible phototuning of Rashba spin-charge converter

The advantage of using SAMs for tailoring the spintronic device is that further functionalities can be incorporated into the spin-orbit device using functional molecules as organic components. The above experimental results suggest the possibility of phototuning the Rashba-Edelstein effect using light-driven molecular transformations. Among many classes of light-switchable molecules, AZs, which can reversibly isomerize between trans and cis forms under the influence of light, have been of great interest because the dipole moment can be tuned with chemistry and are photochemically stable. Here, we have designed an AZ-containing SAM (AZ-SAM) (33, 34) on the Bi/Ag/CoFeB trilayer, shown in Fig. 4A (for details, see Methods). To induce the molecular transformation of the AZ-SAM, we irradiated the AZ-SAM-decorated Bi/Ag/CoFeB trilayer with ultraviolet (UV) light using an ultrahigh-pressure mercury lamp (filtered light, 6.5 mW cm⁻² with $\lambda_{\text{max}} = 360$ nm wavelength) or visible light using a xenon lamp (45 mW cm⁻² with $\lambda = 400$ to 700 nm wavelength) for 3 min. After the irradiation, we measured the ADMR for the Bi/Ag/CoFeB trilayer decorated with the AZ-SAM without irradiation at room temperature.

Figure 4B shows the REMR ratio obtained from the ADMR, $\text{MR} \equiv [\Delta R(\beta = 0) - \Delta R(\beta = 90^\circ)]/R$, for the Bi/Ag/CoFeB decorated with the AZ-SAM after the visible ($N = 1, 3, 5$) or UV ($N = 2, 4$) light irradiation, where N represents the cycle index. Figure 4B demonstrates reversible switching of the REMR ratio by alternating the UV and visible light irradiation; the REMR ratio decreases after the UV light irradiation, whereas it increases after the visible light irradiation, repeatedly. It is notable that the molecular structure of the AZ-SAM is changed by the

irradiation from trans to cis (UV light) and from cis to trans (visible light) (see Fig. 4A). To verify that the observed light-induced REMR modulation is caused by the light-driven molecular transformation, we performed the same measurements on the pristine Bi/Ag/CoFeB trilayer. In the pristine Bi/Ag/CoFeB trilayer, as shown in Fig. 4C, the REMR ratio is not affected by the UV and visible light irradiation. This result demonstrates that the reversible switching of the REMR ratio shown in Fig. 4B originates from the light-driven molecular transformation of the photoswitchable AZ-SAM formed on the Bi/Ag/CoFeB trilayer.

For macroscopic characterization of the trilayer decorated with the AZ-SAM, the static water contact angle θ_s was measured by putting 1.5 μl of a water droplet on the AZ-SAM surface. As shown in Fig. 4D, the water contact angle changes reversibly with the UV and visible light irradiation, providing evidence for the reversible transformations of the AZ-SAM between the two distinct states. The change in the contact angle is partly due to the change in the dipole moment of AZ induced by the cis-trans transformation (see Fig. 4A). In the Bi/Ag/CoFeB trilayer decorated with the AZ-SAM, because of the opposite direction of the dipole between the trans and cis states, the light-driven molecular transformation reverses the direction of the charge transfer at the organic-inorganic interface (35), resulting in the phototuning of the REMR ratio. The sign of the change in the REMR ratio, associated with the direction of the dipole moment, is consistent with the REMR results for the Bi/Ag/CoFeB trilayer decorated with ODT and PFDT (see Figs. 1E, 2, B and C, and 4, A and B).

DISCUSSION

Organic materials are believed to be promising for spintronic applications, benefited from the unlimited versatility of organic materials synthesis. The field of organic spintronics, focused on studying spin relaxation and transport in organic materials, has developed into an attractive field with rich physics. However, few studies have focused on the influence of organic layers on spintronic devices; the spintronic phenomena affected by the formation of organic layers have been largely unexplored. This is in stark contrast to electronics, where the organic functionalization of electronic devices has been extensively

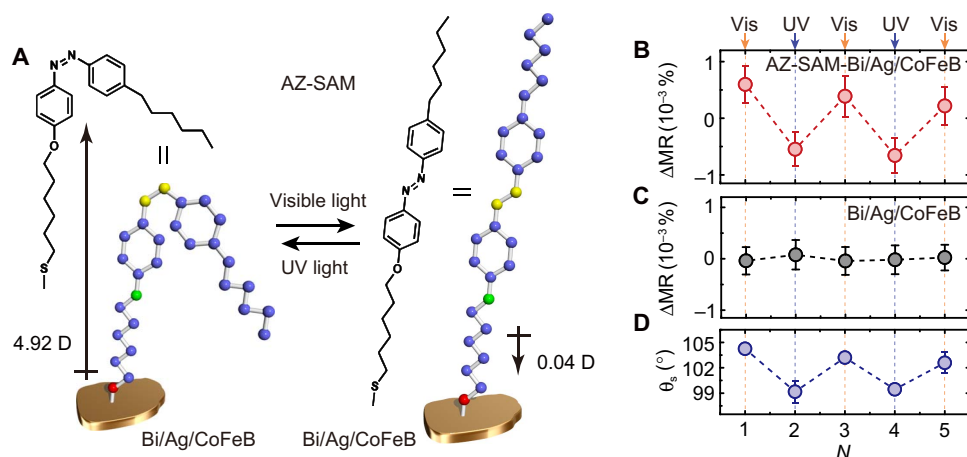


Fig. 4. Phototuning of REMR. (A) Illustration of the reversible cis-trans photoisomerization of AZ-SAM formed on the Bi/Ag/CoFeB trilayer under the UV and visible light irradiation. The arrows represent the dipole moment of AZ obtained from DFT calculations. (B) Change in the REMR ratio $\Delta MR = MR - MR_{avg}$ obtained from the ADMR for the AZ-SAM-decorated Bi/Ag/CoFeB trilayer measured after the visible ($N = 1, 3, 5$) or UV ($N = 2, 4$) light irradiation. Here, $MR = [\Delta R(\beta = 0) - \Delta R(\beta = 90^\circ)]/R$, where N represents the cycle index. MR_{avg} is the average MR for $N = 1, 2, 3, 4, 5$. (C) REMR ratio for the pristine Bi/Ag/CoFeB trilayer measured after the visible ($N = 1, 3, 5$) or UV ($N = 2, 4$) light irradiation. (D) Static water contact angle θ_s for the AZ-SAM-decorated Bi/Ag/CoFeB trilayer measured after the visible ($N = 1, 3, 5$) or UV ($N = 2, 4$) light irradiation.

studied in the literature. Here, contrary to the previous works, we used organic monolayers to tailor spintronic phenomena in metallic heterostructures, which enabled to design the functionalized spin-orbit devices. Therefore, our work not only demonstrates the molecular engineering of the Rashba spin-orbit devices but also provides a new avenue for harnessing organic materials in spintronics, opening a new direction of organic spintronics. We also note that the tuning of the spin-charge interconversion has been achieved by applying a gate voltage in spintronic devices based on oxides (36), graphene (37), and topological insulators (38). The molecular engineering provides a new way to tune the spin-orbit phenomenon in solid-state devices.

METHODS

SAM formation on spin-orbit devices

ODT and PFDT were dissolved into ethanol with a concentration of 2 mM. 6-(4-((4-Hexylphenyl)diazanyl)phenoxy)hexane-1-thiol (the azobenzene molecule) was dissolved into dichloromethane with 1 mM. The Bi/Ag/CoFeB trilayer films were immersed into the solution for 20 hours. All processes were performed at room temperature.

Synthesis of AZ compound

4-((4-Hexylphenyl)diazanyl)phenol (1)

4-Hexylaniline (3.86 g, 21.8 mmol) was dissolved in a mixture of concentrated hydrochloric acid (4 ml) and water (25 ml). Sodium nitrate (1.89 g, 27.3 mmol) in water (3 ml) was added dropwise to the above solution below 5°C. Aqueous solution (130 ml) dissolving phenol (2.51 g, 26.7 mmol) and sodium hydroxide (1.34 g, 33.5 mmol) were then added dropwise under vigorous stirring. The reaction mixture were stirred for 2 hours below 5°C and for 3 hours at room temperature. After neutralization with diluted hydrochloric acid, the precipitate was filtered off and dissolved in ethyl acetate. The solution was washed with brine and dried over anhydrous sodium sulfate. The solvent was removed under reduced pressure and the residue was then recrystallized from hexane to afford **1** (4.85 g, 79%) as an orange solid. $^1\text{H NMR}$ (nuclear magnetic resonance) (400 MHz, CDCl_3) δ [parts per million (ppm)]

7.86 (2H, d, $J = 9.2$ Hz), 7.79 (2H, d, $J = 8.4$ Hz), 7.30 (2H, d, $J = 8.8$ Hz), 6.94 (2H, d, $J = 8.4$ Hz), 5.49 (1H, s), 2.67 (2H, t, $J = 6.8$ Hz), 1.68 to 1.28 (8H, m), 0.89 (3H, t, $J = 6.8$ Hz).

1-(4-((6-Bromohexyl)oxy)phenyl)-2-(4-hexylphenyl)diazene (2)

Potassium carbonate (1.38 g, 10.0 mmol) and a catalytic amount of potassium iodide were added to a mixed solution of **1** (1.41 g, 5.00 mmol) and 1,6-dibromohexane (3.66 g, 15.0 mmol) in dimethylformamide (40 ml), potassium carbonate (1.38 g, 10.0 mmol), and the reaction mixture was stirred overnight at room temperature. The reaction mixture was extracted with diethyl ether. The extract was washed with brine and dried over anhydrous sodium sulfate. After the solvent was removed under reduced pressure, the residue was recrystallized from hexane/ethanol to afford **2** (1.40 g, 63%) as an orange solid. $^1\text{H NMR}$ (400 MHz, CDCl_3) δ (ppm) 7.89 (2H, d, $J = 9.6$ Hz), 7.80 (2H, d, $J = 8.8$ Hz), 7.30 (2H, d, $J = 8.4$ Hz), 7.00 (2H, d, $J = 8.8$ Hz), 4.05 (2H, t, $J = 6.6$ Hz), 3.44 (2H, t, $J = 6.8$ Hz), 2.67 (2H, t, $J = 7.8$ Hz), 1.88 to 1.32 (16H, m), 0.89 (3H, t, $J = 6.9$ Hz).

6-(4-((4-Hexylphenyl)diazanyl)phenoxy)hexane-1-thiol (3)

Synthesis of **3** was performed under nitrogen atmosphere; **2** (0.891 g, 2.00 mmol) and hexamethyldisilathiane (0.506 ml, 2.40 mmol) were dissolved in dry tetrahydrofuran (THF; 20 ml). After cooling to -10°C , tetrabutylammonium fluoride in 1 M THF (2.20 ml, 2.20 mmol) was added dropwise to the mixture. The reaction mixture was stirred for 2 hours at -10°C and overnight at room temperature. The reaction was quenched with saturated aqueous ammonium chloride (20 ml), and the reaction mixture was extracted with chloroform. The extract was washed with brine and dried over anhydrous sodium nitrate. After the solvent was removed under reduced pressure, the residue was recrystallized from ethanol to afford **3** (0.728 g, 91%) as an orange solid. $^1\text{H NMR}$ (400 MHz, CDCl_3) δ (ppm) 7.89 (2H, d, $J = 8.4$ Hz), 7.80 (2H, d, $J = 8.0$ Hz), 7.30 (2H, d, $J = 8.0$ Hz), 6.99 (2H, d, $J = 8.0$ Hz), 4.04 (2H, t, $J = 6.4$ Hz), 2.69 (2H, t, $J = 7.4$ Hz), 2.55 (2H, t, $J = 7.2$ Hz), 1.85 to 1.21 (17H, m), 0.89 (3H, t, $J = 6.8$ Hz) electrospray ionization mass spectrometry (ESI-MS) $[M + H]^+$: calcd for $[M + H]^+$ ($\text{C}_{24}\text{H}_{35}\text{N}_2\text{OS}$) mass/charge ratio (m/z) 399.25, found 399.22.

Materials and instruments

All reagents and solvents were commercially available and used as received. ¹H NMR spectra were recorded on JNM-AL400 (JEOL). ESI-MS spectra were obtained using Mass Spectrometer-LCT Premier/XE (Waters).

Dipole calculation

Dipole moments of the SAM-forming molecules were calculated by DFT calculations with Gaussian 03 at the B3LYP/6-31G* level. The molecular geometries were optimized at the same level.

SUPPLEMENTARY MATERIALS

Supplementary material for this article is available at <http://advances.sciencemag.org/cgi/content/full/4/3/eaar3899/DC1>

section S1. Atomic force microscopy

section S2. Infrared reflection-absorption spectroscopy

section S3. Field ADMR in SAM-decorated Bi/CoFeB bilayers

section S4. Field strength dependence of MR in SAM-decorated Bi/Ag/CoFeB trilayers

section S5. Charge transfer at organic-inorganic interface

fig. S1. AFM images of the Bi/Ag/CoFeB trilayer and SAM-decorated Bi/Ag/CoFeB trilayers.

fig. S2. IRRAS spectra of SAM-decorated Bi/Ag/CoFeB trilayers and infrared absorption spectra of bulk materials.

fig. S3. Field ADMR in SAM-decorated Bi/CoFeB bilayers.

fig. S4. Charge transfer at organic-inorganic interface.

table S1. Field strength dependence of MR.

REFERENCES AND NOTES

- I. M. Miron, K. Garello, G. Gaudin, P.-J. Zermatten, M. V. Costache, S. Auffret, S. Bandiera, B. Rodmacq, A. Schuhl, P. Gambardella, Perpendicular switching of a single ferromagnetic layer induced by in-plane current injection. *Nature* **476**, 189–193 (2011).
- L. Liu, C.-F. Pai, Y. Li, H. Tseng, D. Ralph, R. Buhrman, Spin-torque switching with the giant spin Hall effect of tantalum. *Science* **336**, 555–558 (2012).
- G. Yu, P. Upadhyaya, Y. Fan, J. G. Alzate, W. Jiang, K. L. Wong, S. Takei, S. A. Bender, L.-T. Chang, Y. Jiang, M. Lang, J. Tang, Y. Wang, Y. Tserkovnyak, P. K. Amiri, K. L. Wang, Switching of perpendicular magnetization by spin-orbit torques in the absence of external magnetic fields. *Nat. Nanotechnol.* **9**, 548–554 (2014).
- H. Kurebayashi, J. Sinova, D. Fang, A. Irvine, T. Skinner, J. Wunderlich, V. Novák, R. Campion, B. Gallagher, E. Vehstedt, L. P. Žárbo, K. Výborný, A. J. Ferguson, T. Jungwirth, An antidamping spin-orbit torque originating from the Berry curvature. *Nat. Nanotechnol.* **9**, 211–217 (2014).
- S. Fukami, C. Zhang, S. DuttaGupta, A. Kurenkov, H. Ohno, Magnetization switching by spin-orbit torque in an antiferromagnet-ferromagnet bilayer system. *Nat. Mater.* **15**, 535–541 (2016).
- A. Manchon, H. C. Koo, J. Nitta, S. M. Frolov, R. A. Duine, New perspectives for Rashba spin-orbit coupling. *Nat. Mater.* **14**, 871–882 (2015).
- A. Soumyanarayanan, N. Reyren, A. Fert, C. Panagopoulos, Emergent phenomena induced by spin-orbit coupling at surfaces and interfaces. *Nature* **539**, 509–517 (2016).
- A. Hoffmann, Spin Hall effects in metals. *IEEE Trans. Magn.* **49**, 5172–5193 (2013).
- J. Sinova, S. O. Valenzuela, J. Wunderlich, C. H. Back, T. Jungwirth, Spin Hall effects. *Rev. Mod. Phys.* **87**, 1213–1260 (2015).
- Y. Niimi, Y. Otani, Reciprocal spin Hall effects in conductors with strong spin-orbit coupling: A review. *Rep. Prog. Phys.* **78**, 124501 (2015).
- T. Jungwirth, J. Wunderlich, K. Olejník, Spin Hall effect devices. *Nat. Mater.* **11**, 382–390 (2012).
- E. I. Rashba, Properties of semiconductors with an extremum loop. 1. Cyclotron and combination resonance in a magnetic field perpendicular to the plane of the loop. *Sov. Phys. Solid State* **2**, 1109–1122 (1960).
- V. M. Edelstein, Spin polarization of conduction electrons induced by electric current in two-dimensional asymmetric electron systems. *Solid State Commun.* **73**, 233–235 (1990).
- Y. K. Kato, R. C. Myers, A. C. Gossard, D. D. Awschalom, Current-induced spin polarization in strained semiconductors. *Phys. Rev. Lett.* **93**, 176601 (2004).
- P. Gambardella, I. M. Miron, Current-induced spin-orbit torques. *Philos. Trans. A Math. Phys. Eng. Sci.* **369**, 3175–3197 (2011).
- S. Onclon, B. J. Ravoo, D. N. Reinhoudt, Engineering silicon oxide surfaces using self-assembled monolayers. *Angew. Chem. Int. Ed.* **44**, 6282–6304 (2005).
- B. de Boer, A. Hadjipour, M. M. Mandoc, T. van Woudenberg, P. W. M. Blom, Tuning of metal work functions with self-assembled monolayers. *Adv. Mater.* **17**, 621–625 (2005).
- J. H. Fendler, Chemical self-assembly for electronic applications. *Chem. Mater.* **13**, 3196–3210 (2001).
- H. Ma, H.-L. Yip, F. Huang, A. K.-Y. Jen, Interface engineering for organic electronics. *Adv. Funct. Mater.* **20**, 1371–1388 (2010).
- J. C. Love, L. A. Estroff, J. K. Kriebel, R. G. Nuzzo, G. M. Whitesides, Self-assembled monolayers of thiolates on metals as a form of nanotechnology. *Chem. Rev.* **105**, 1103–1170 (2005).
- A. Ulman, Formation and structure of self-assembled monolayers. *Chem. Rev.* **96**, 1533–1554 (1996).
- C. R. Ast, J. Henk, A. Ernst, L. Moerschini, M. C. Falub, D. Pacilé, P. Bruno, K. Kern, M. Grioni, Giant spin splitting through surface alloying. *Phys. Rev. Lett.* **98**, 186807 (2007).
- H. Nakayama, Y. Kanno, H. An, T. Tashiro, S. Haku, A. Nomura, K. Ando, Rashba-Edelstein magnetoresistance in metallic heterostructures. *Phys. Rev. Lett.* **117**, 116602 (2016).
- H. Ron, H. Cohen, S. Matlis, M. Rappaport, I. Rubinstein, Self-assembled monolayers on oxidized metals. 4. Superior *n*-alkanethiol monolayers on copper. *J. Phys. Chem. B* **102**, 9861–9869 (1998).
- W. Gil, D. Görliitz, M. Horisberger, J. Kötzler, Magnetoresistance anisotropy of polycrystalline cobalt films: Geometrical-size and domain effects. *Phys. Rev. B* **72**, 134401 (2005).
- D. Cahen, R. Naaman, Z. Vager, The cooperative molecular field effect. *Adv. Funct. Mater.* **15**, 1571–1578 (2005).
- V. S. Edel'man, Properties of electrons in bismuth. *Sov. Phys. Usp.* **20**, 819–835 (1977).
- H. Ishii, K. Sugiyama, E. Ito, K. Seki, Energy level alignment and interfacial electronic structures at organic/metal and organic/organic interfaces. *Adv. Mater.* **11**, 605–625 (1999).
- F. B. de Mongeot, A. Cupolillo, M. Rocca, U. Valbusa, Sub-surface incorporation of oxygen on Ag (001) during molecular dissociation. *Chem. Phys. Lett.* **302**, 302–306 (1999).
- Y. Tserkovnyak, A. Brataas, G. E. W. Bauer, B. I. Halperin, Nonlocal magnetization dynamics in ferromagnetic heterostructures. *Rev. Mod. Phys.* **77**, 1375–1421 (2005).
- J. C. Rojas-Sánchez, L. Vila, G. Desfonds, S. Gambarelli, J. Attané, J. De Teresa, C. Magén, A. Fert, Spin-to-charge conversion using Rashba coupling at the interface between non-magnetic materials. *Nat. Commun.* **4**, 2944 (2013).
- E. Saitoh, M. Ueda, H. Miyajima, G. Tatara, Conversion of spin current into charge current at room temperature: Inverse spin-Hall effect. *Appl. Phys. Lett.* **88**, 182509 (2006).
- T. Kobayashi, T. Seki, Odd-even effects in Azobenzene-urea amphiphile assemblies. *Langmuir* **19**, 9297–9304 (2003).
- J. Hu, M. A. Fox, A convenient trimethylsilylthioxy-dehalogenation reaction for the preparation of functionalized thiols. *J. Org. Chem.* **64**, 4959–4961 (1999).
- M. Suda, N. Kameyama, A. Ikegami, Y. Einaga, Reversible phototuning of the large anisotropic magnetization at the interface between a self-assembled photochromic monolayer and gold. *J. Am. Chem. Soc.* **131**, 865–870 (2009).
- E. Lesne, Y. Fu, S. Oyarzun, J. Rojas-Sánchez, D. Vaz, H. Naganuma, G. Sicoli, J.-P. Attané, M. Jamet, E. Jacquet, J.-M. George, A. Barthélémy, H. Jaffrès, A. Fert, M. Bibes, L. Vila, Highly efficient and tunable spin-to-charge conversion through Rashba coupling at oxide interfaces. *Nat. Mater.* **15**, 1261–1266 (2016).
- S. Dushenko, H. Ago, K. Kawahara, T. Tsuda, S. Kuwabata, T. Takenobu, T. Shinjo, Y. Ando, M. Shiraishi, Gate-tunable spin-charge conversion and the role of spin-orbit interaction in graphene. *Phys. Rev. Lett.* **116**, 166102 (2016).
- Y. Fan, X. Kou, P. Upadhyaya, Q. Shao, L. Pan, M. Lang, X. Che, J. Tang, M. Montazeri, K. Murata, L.-T. Chang, M. Akyol, G. Yu, T. Nie, K. L. Wong, J. Liu, Y. Wang, Y. Tserkovnyak, K. L. Wang, Electric-field control of spin-orbit torque in a magnetically doped topological insulator. *Nat. Nanotechnol.* **11**, 352–359 (2016).
- M. D. Porter, T. B. Bright, D. L. Allara, C. E. D. Chidsey, Spontaneously organized molecular assemblies. 4. Structural characterization of *n*-alkyl thiol monolayers on gold by optical ellipsometry, infrared spectroscopy, and electrochemistry. *J. Am. Chem. Soc.* **109**, 3559–3568 (1987).
- G. Floß, G. Granucci, P. Saalfrank, Surface hopping dynamics of direct *trans* → *cis* photoswitching of an azobenzene derivative in constrained adsorbate geometries. *J. Chem. Phys.* **137**, 234701 (2012).

Acknowledgments: We thank K. Fukuda of RIKEN and T. Minami and S. Watanabe of the University of Tokyo for stimulating discussions. We also thank JASCO for helping with the IRRAS measurements. **Funding:** This work was supported by Japan Society for the Promotion of Science KAKENHI grant numbers 26220604, 26103004, 17H04808, and 17F17066; PRESTO-JST Agency “Innovative nano-electronics through interdisciplinary

collaboration among material, device and system layers” grant number 13415036; the Mitsubishi Foundation; the Asahi Glass Foundation; the Mizuho Foundation for the Promotion of Sciences; the Casio Science Promotion Foundation; the Murata Science Foundation; and Spintronics Research Network of Japan (Spin-RNJ). **Author contributions:** H.N., H.A., and K.T. fabricated the devices. H.N. collected and analyzed the data. K.A., H.N., T.Y., and Y.E. designed the experiments and developed the explanation. K.A., H.N., and T.Y. wrote the manuscript. All authors discussed the results and reviewed the manuscript. H.N. claims the responsibility for all the figures in the main text and the Supplementary Materials. **Competing interests:** The authors declare that they have no competing interests. **Data and materials availability:** All data needed to evaluate the

conclusions in the paper are present in the paper and/or the Supplementary Materials. Additional data related to this paper may be requested from the authors.

Submitted 2 November 2017

Accepted 10 February 2018

Published 23 March 2018

10.1126/sciadv.aar3899

Citation: H. Nakayama, T. Yamamoto, H. An, K. Tsuda, Y. Einaga, K. Ando, Molecular engineering of Rashba spin-charge converter. *Sci. Adv.* **4**, eaar3899 (2018).